catalysts

MDPI

Article

Synergistic Effect of Physicochemical Properties of Ni Nanofibrous Catalysts on Catalytic Performance for Methane Partial Oxidation

Yuyao Ma [1,2,*], Yongtao Wang [1,2] and Wenqing Wei [1,2]

[1] School of Mechanical and Automation, Weifang University, Weifang 261061, China; yongtao-wang@hotmail.com (Y.W.); hitweiwenqing@126.com (W.W.)
[2] Shandong Key Laboratory of Intelligent Manufacturing Technology for Advanced Power Equipment, Weifang 261061, China
* Correspondence: 20220032@wfu.edu.cn; Tel.: +86-183-6610-7880

Abstract

For supported catalysts, the synergistic effect of physicochemical properties (including oxygen storage capacity (OSC), metal–support interaction, dispersion, and reducibility) is crucial for methane partial oxidation (POM). This study aims to prepare Ni-based nanofibrous catalysts using traditional metal oxides (Al_2O_3, ZrO_2, CeO_2, $Zr_{0.92}(Y_2O_3)_{0.08}O_{2-\delta}$, and $Ce_{0.9}Gd_{0.1}O_{2-\delta}$) as supports via electrospinning, and thoroughly investigates the synergistic effect of the catalyst's physicochemical properties on catalytic performance. For the $Ni/Zr_{0.92}(Y_2O_3)_{0.08}O_{2-\delta}$ and $Ni/Ce_{0.9}Gd_{0.1}O_{2-\delta}$ catalysts, doping significantly enhances Ni dispersion, reducibility, and OSC, thereby improving catalytic performance. The results demonstrate that the catalytic activity follows the following order: $Ni/Ce_{0.9}Gd_{0.1}O_{2-\delta} > Ni/CeO_2 > Ni/Zr_{0.92}(Y_2O_3)_{0.08}O_{2-\delta} > Ni/ZrO_2 > Ni/Al_2O_3$, which is closely associated with the synergistic effect of their physicochemical properties. In addition, this study focuses on elucidating the underlying mechanism by which the Gd^{3+} doping level influences the catalytic performance of the $Ni/Ce_{0.9}Gd_xO_{2-\delta}$ (x = 0.1, 0.2, 0.3) catalysts. The $Ni/Ce_{0.9}Gd_{0.1}O_{2-\delta}$ catalyst exhibits the optimal Ni dispersion, reducibility, and OSC, corresponding to the highest catalytic performance. This re-emphasizes the crucial role of the synergistic effect of the catalyst's physicochemical properties in determining catalytic performance. Therefore, investigating this synergistic effect is essential for achieving superior catalytic performance.

Keywords: nanofibrous catalysts; physicochemical properties; synergistic effect; doping; methane partial oxidation

check for updates

Academic Editor: Valeria La Parola

Received: 26 October 2025
Revised: 15 November 2025
Accepted: 18 November 2025
Published: 19 November 2025

Citation: Ma, Y.; Wang, Y.; Wei, W. Synergistic Effect of Physicochemical Properties of Ni Nanofibrous Catalysts on Catalytic Performance for Methane Partial Oxidation. *Catalysts* **2025**, *15*, 1090. https://doi.org/10.3390/catal15111090

Copyright: © 2025 by the authors. Licensee MDPI, Basel, Switzerland. This article is an open access article distributed under the terms and conditions of the Creative Commons Attribution (CC BY) license (https://creativecommons.org/licenses/by/4.0/).

1. Introduction

For supported catalysts, the support plays an important role in the catalytic reaction because it provides certain physicochemical properties, such as oxygen storage capacity (OSC), metal–support interaction, dispersion, and reducibility [1–5]. The metal–support interaction affects the dispersion and reducibility of the active metal, which further affects the catalytic activity [6,7]. For example, $NiAl_2O_4$ spinel, the strong interaction between Ni and support improves the dispersion but reduces the reducibility of Ni [8,9]. However, supports with high OSC can promote reducibility [4,10]. In addition, the oxygen stored in the support also participates in the reaction [11,12]. Therefore, the OSC of the support has a significant effect on the catalyst activity. It is related to the formation of oxygen vacancies

along with their diffusion ability in supports [13,14], which can be further enhanced by incorporating dopants into the support lattice [14,15]. Additionally, the dopant as an obstacle can also prevent the aggregation of active sites [16], and therefore improve the dispersion of the active sites. Studies by Dong et al. [11] have shown that the key step in the methane partial oxidation (POM) reaction is the methane decomposition ($CH_4 \rightarrow CH_x$), followed by the oxidation of CH_x radicals to form CO. This indicates that the OSC of the support helps to promote CH_4 conversion to syngas. Therefore, the synergistic effect of the physicochemical properties of catalysts is crucial for POM.

Ni is the most commonly used active metal for catalyst owing to its low cost and high activity [15,17]. Al_2O_3, ZrO_2 and CeO_2 are common supports in Ni catalysts [18–21]. The inert Al_2O_3 support has no OSC, but it improves dispersion and reduces reducibility. ZrO_2 is prone to form defects and surface oxygen vacancies [22,23]. When the trivalent rare earth element ion (e.g., Y^{3+}, Ce^{3+}, La^{3+} and Sm^{3+}) is doped, oxygen vacancies will be formed in the ZrO_2 lattice to maintain electroneutrality, which increases the OSC of the support [24]. Charisiou et al. [10] proved that adding Y_2O_3 to the ZrO_2 support not only enhanced the OSC of the support, but also improved the dispersion and reducibility of Ni. CeO_2 is more active and is known for its oxygen mobility and storage capacity. Moreover, the OSC of CeO_2 in SOFC can be further improved through Gd^{3+} doping [25]. It was reported that the OSC of the support affects the catalytic activity, especially the introduction of oxygen vacancies by doping, which can enhance the catalytic activity [12,26,27]. Some authors have conducted studies on the effect of traditional supports on the dispersion and reducibility of Ni [28,29]. However, differences in the specific surface area of supports, resulting from variations in their preparation methods, raw materials, and sintering activity, can obscure the impacts of dispersion and reducibility on catalytic performance. Furthermore, previous studies have mainly focused on macroscopic catalytic performance, while the synergistic effects between physicochemical properties have been insufficiently explored. More importantly, these studies have not addressed the influence exerted by the OSC of different supports. In summary, the synergistic effect of the physicochemical properties of different supports (including OSC, metal–support interaction, dispersion, and reducibility) on the performance of POM has not yet been clearly demonstrated.

Electrospinning is an effective method for producing fibrous catalysts with controllable diameters from 50 nm to 1 μm [21,30]. To eliminate the interference of differences in specific surface area on the core research conclusions, the specific surface areas of all target catalysts were maintained consistent by adjusting the fiber diameter. Simultaneously, the fibrous catalyst exhibits high thermal stability, ensuring structural integrity and resistance to sintering [1,31]. In addition, the fibrous structure has the morphological advantage of easily distinguishing Ni from the support [32]. Under this premise, this study aims to fabricate Ni-based fibrous catalysts using traditional metal oxides—including Al_2O_3, ZrO_2, CeO_2, $Zr_{0.92}(Y_2O_3)_{0.08}O_{2-\delta}$ (Y^{3+}-doped ZrO_2), and $Ce_{0.9}Gd_{0.1}O_{2-\delta}$ (Gd^{3+}-doped CeO_2)—as supports, and thoroughly investigates the synergistic effect of the physicochemical properties of different supports on catalytic performance. Moreover, this study also focused on investigating the effects of different Gd^{3+} doping contents on the physicochemical properties of $Ni/Ce_{0.9}Gd_xO_{2-\delta}$ (x = 0.1, 0.2, 0.3) catalysts, and further clarified their impacts on catalytic performance. This provides new theoretical basis and design strategies for the rational design of next-generation POM catalysts.

2. Results

2.1. Comparison of Different Supported Catalysts

2.1.1. XRD Analysis

Different supports can affect crystallite size; thus, all catalysts were subjected to XRD analysis. Figure 1a shows the XRD patterns of all catalysts after reduction. Figure 1b shows a partially enlarged view of Figure 1a, and Ni peak was detected at $2\theta \approx 44.5^{\circ}$. For the Ni/Al_2O_3 catalyst, the formation of $NiAl_2O_4$ spinel leads to a strong interaction between Ni and support, which inhibits Ni crystal growth. Therefore, the intensity of the Ni peak is broad and less intense. Ni/CeO_2 and Ni/ZrO_2 catalysts did not form new phases. Therefore, the interaction between Ni and supports is weak, which results in a large Ni crystallite size. After doping CeO_2 with Gd^{+3}, both CeO_2 and the resulting $Ce_{0.9}Gd_{0.1}O_{2-\delta}$ retained the cubic fluorite structure. However, in the case of the $Ni/Ce_{0.9}Gd_{0.1}O_{2-\delta}$ catalyst, all diffraction peaks exhibited lower intensity compared to those of Ni/CeO_2, suggesting a reduction in crystallite size. Therefore, the Ni crystallite size also decreases. Doping ZrO_2 with Y_2O_3, Y^{+3} ions dissolved in the lattice of ZrO_2, replacing some Zr^{+4} ions at the lattice site to form a new cubic phase $Zr_{0.92}(Y_2O_3)_{0.08}O_{2-\delta}$. For the $Ni/Zr_{0.92}(Y_2O_3)_{0.08}O_{2-\delta}$ catalyst, no Ni peak was detected, indicating that after doping the Ni dispersion was improved and amorphous Ni was formed. This may be responsible for dopants hinder Ni crystal growth and interfere with crystallization [22]. Indeed, doping inhibits Ni crystal growth.

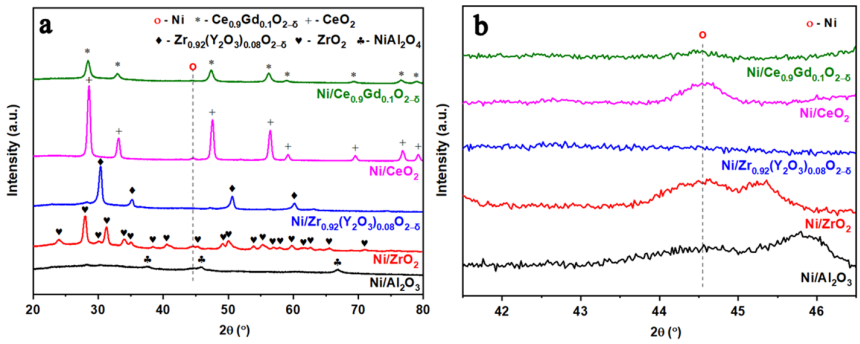


Figure 1. XRD patterns of the reduced catalysts (**a**) and partially enlarged (**b**).

2.1.2. Microstructure Analysis

The fibrous catalyst exhibited high thermal stability, which can ensure the structure stability of the catalyst and is not affected by sintering. As shown in Figure 2, all the catalysts retained the fibrous structure with similar fiber diameters (≈300 nm), and their specific surface areas ranged from 33 to 35 $m^2 \cdot g^{-1}$, ensuring the consistency of the specific surface area as a variable. However, the particle size and texture of the fibrous catalyst surface are significantly different, which may cause different dispersion. For the Ni/Al_2O_3 catalyst, the formation of $NiAl_2O_4$ leads to a smooth surface of the support. For the doped $Ni/Zr_{0.92}(Y_2O_3)_{0.08}O_{2-\delta}$ catalyst, the surface texture becomes fine. For the doped $Ni/Ce_{0.9}Gd_{0.1}O_{2-\delta}$ catalyst, the surface particle size decreases. In order to further clearly observe the Ni dispersion of the catalyst, TEM and EDS characterization results are shown in Figure 3. It can be seen that Ni particles are highly dispersed on the surface of the $NiAl_2O_4$ support due to the strong interaction. There is obvious Ni aggregation on the surface of ZrO_2 and CeO_2 supports. Notably, for both the $Ni/Zr_{0.92}(Y_2O_3)_{0.08}O_{2-\delta}$ and $Ni/Ce_{0.9}Gd_{0.1}O_{2-\delta}$ catalysts, it is intuitively shown that doping significantly improves the Ni dispersion. The above results are consistent with the XRD results. That is, doping inhibits the growth and aggregation of Ni, thereby improving the dispersion.

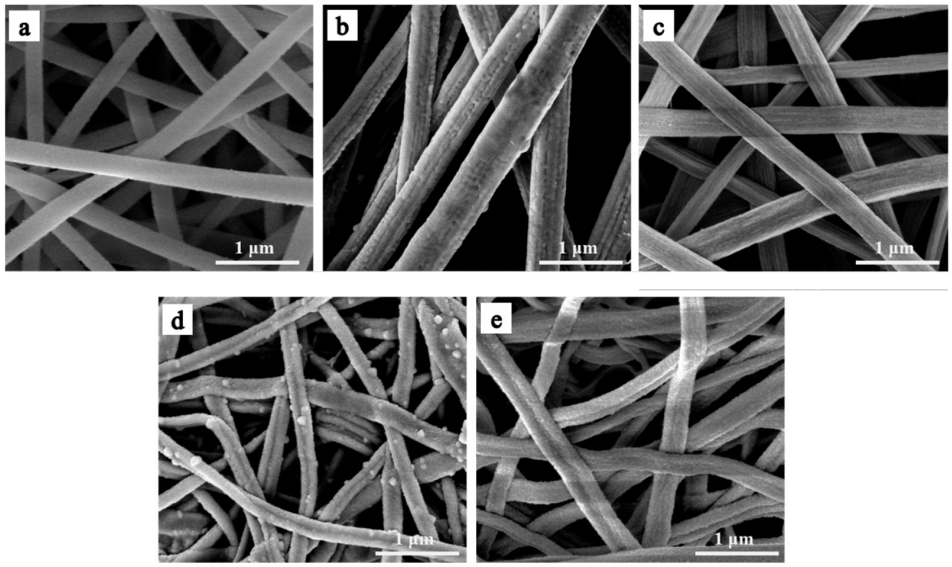


Figure 2. SEM images of the reduced catalysts: (**a**) Ni/Al_2O_3; (**b**) Ni/ZrO_2; (**c**) $Ni/Zr_{0.92}(Y_2O_3)_{0.08}O_{2-\delta}$; (**d**) Ni/CeO_2; (**e**) $Ni/Ce_{0.9}Gd_{0.1}O_{2-\delta}$.

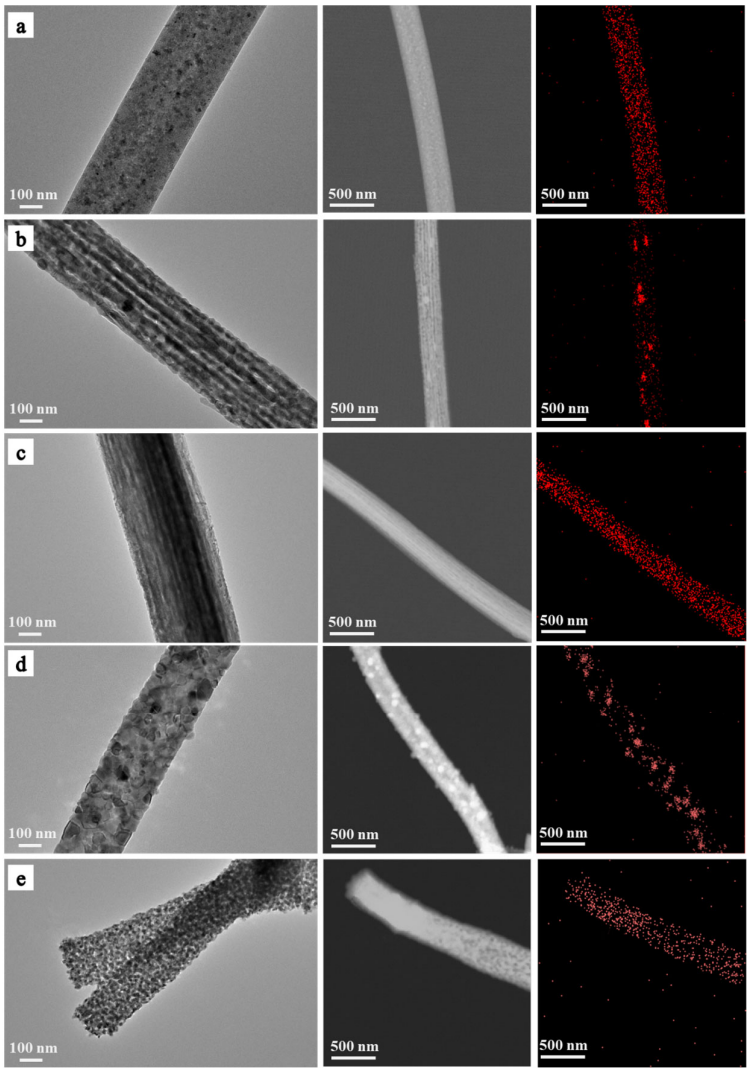


Figure 3. TEM images (**left**) and corresponding EDS Ni mapping (**right**) of reduced catalysts with different supports: (**a**) Ni/Al_2O_3; (**b**) Ni/ZrO_2; (**c**) $Ni/Zr_{0.92}(Y_2O_3)_{0.08}O_{2-\delta}$; (**d**) Ni/CeO_2; (**e**) $Ni/Ce_{0.9}Gd_{0.1}O_{2-\delta}$.

2.1.3. Reducibility and Dispersion Analysis

TPR analysis was carried out to determine the reducibility and interaction between Ni and supports. Different peaks are associated with different interactions between NiO and support. The strong interaction leads to the shift in reduction peak to high temperatures, while the weak interaction results in reduction at low temperatures. As shown in Figure 4, the Ni/Al_2O_3 catalyst exhibited a reduction peak at 800 °C, indicating a strong metal–support interaction. This interaction is attributed to its lowest reducibility, as presented in Table 1. The Ni/ZrO_2 catalyst presented two reduction peaks at 380 °C and 625 °C, indicating weak and strong interactions between Ni and the support. The reduction peaks of $Ni/Zr_{0.92}(Y_2O_3)_{0.08}O_{2-\delta}$ catalyst doped with Y^{3+} both shifted to low temperature. On one hand, the reduction process is facilitated by the decreased crystallite size. On the other hand, the increased oxygen vacancies strongly interact with the adjacent oxygen in NiO, thereby weakening the Ni-O bond [10,22]. Consequently, NiO becomes more readily reducible, leading to enhanced catalyst reducibility. For the Ni/CeO_2 catalyst, the peak at 338 °C is attributed to NiO reduction, while the peak at 780 °C is related to CeO_2 reduction [33,34]. After Gd^{3+} doping, the Ni reducibility of $Ni/Ce_{0.9}Gd_{0.1}O_{2-\delta}$ catalyst was also slightly increased. In other words, doping is conducive to improving the reducibility.

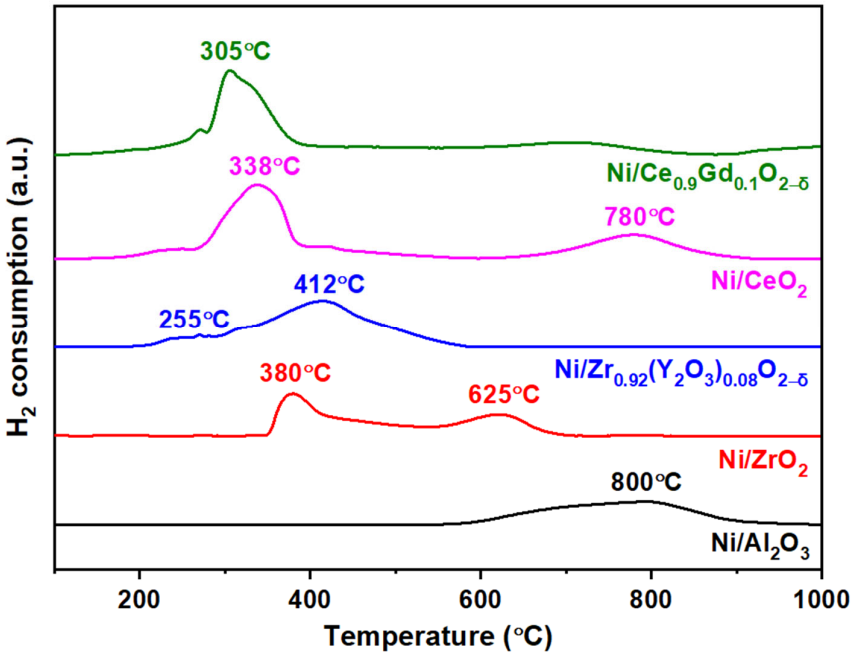


Figure 4. TPR profiles of the catalysts.

Table 1. Physicochemical properties of the catalysts.

Samples	Reducibility (%)	Dispersion (%)	OSC (mmol $g^{-1}_{support}$)
Ni/Al_2O_3	59.1	13.4	0.0
Ni/ZrO_2	69.0	9.5	3.4
$Ni/Zr_{0.92}(Y_2O_3)_{0.08}O_{2-\delta}$	93.3	31.4	20.5
Ni/CeO_2	93.5	n.a.	32.0
$Ni/Ce_{0.9}Gd_{0.1}O_{2-\delta}$	95.5	n.a.	45.1

n.a.: Not analyzed.

CO-TPD analysis was performed to evaluate the Ni dispersion of the catalysts, and the results are listed in Table 1. The low reducibility of the Ni/Al_2O_3 catalyst results

in its low dispersion. Due to the interference of Ce, the dispersion of Ni/CeO_2 and $Ni/Ce_{0.9}Gd_{0.1}O_{2-\delta}$ catalysts was not analyzed. Y^{3+} doping improved the Ni dispersion of $Ni/Zr_{0.92}(Y_2O_3)_{0.08}O_{2-\delta}$ catalyst, which was consistent with the TEM and EDS results. Therefore, doping can improve the dispersion of active sites.

2.1.4. Measurement of Support OSC

Considering the importance of the OSC of the catalyst during the POM, O_2-TPD was used to analyze the OSC of different supports. As shown in Figure 5, there are two kinds of O_2 desorption peaks: physical adsorption in low temperature region (<600 °C) and chemical adsorption in high temperature region (>600 °C) [35]. However, the OSC refers to chemical adsorption. Therefore, only the high temperature region was integrated, and the results are listed in Table 1. The Al_2O_3 support has almost no OSC. The ZrO_2 support exhibits relatively weak OSC, but doping with Y^{3+} can introduce oxygen vacancies into the lattice to enhance OSC [10]. CeO_2 itself can undergo strong redox reactions, so the OSC of the CeO_2 support is higher than that of the Y^{3+}-doped $Zr_{0.92}(Y_2O_3)_{0.08}O_{2-\delta}$ support. The Gd^{3+}-doped $Ce_{0.9}Gd_{0.1}O_{2-\delta}$ support exhibits the highest OSC [25], indicating that doping can enhance the OSC of supports.

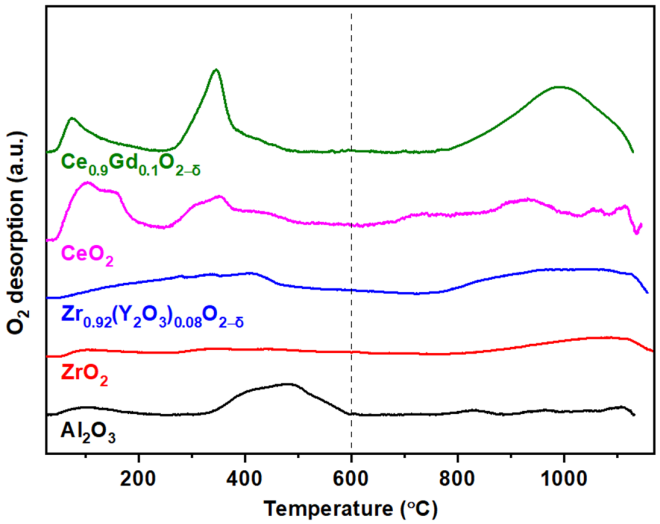


Figure 5. O_2-TPD profiles of different supports.

2.1.5. Catalytic Performance

It can be seen from the above results that the dispersion, reducibility, and OSC of different supported catalysts exhibit differences. The synergistic effect of the physicochemical properties of catalysts on catalytic performance at different reaction temperatures is shown in Figure 6. For the Ni/Al_2O_3 catalyst, although the Ni dispersion is good, while the reducibility is the lowest and the support has little OSC. In addition, the low Ni content is readily oxidized to inactive $NiAl_2O_4$ during the POM [32]. Therefore, the catalytic activity of the Ni/Al_2O_3 catalyst is the lowest. As was mentioned, for Ni/ZrO_2 and Ni/CeO_2 catalysts, doping improves the OSC, dispersion, and reducibility of the catalysts. Therefore, the performance of the $Ni/Zr_{0.92}(Y_2O_3)_{0.08}O_{2-\delta}$ and $Ni/Ce_{0.9}Gd_{0.1}O_{2-\delta}$ catalysts is higher than that of the corresponding un-doped catalysts, respectively. The Ni/CeO_2 and $Ni/Zr_{0.92}(Y_2O_3)_{0.08}O_{2-\delta}$ catalysts exhibit similar reducibility. TEM and EDS analysis results show that the Ni dispersion in the Ni/CeO_2 catalyst is lower than that in the $Ni/Zr_{0.92}(Y_2O_3)_{0.08}O_{2-\delta}$ catalyst, but the OSC of the CeO_2 support is higher than that of the $Zr_{0.92}(Y_2O_3)_{0.08}O_{2-\delta}$ support. Ultimately, the Ni/CeO_2 catalyst slightly outperforms the $Ni/Zr_{0.92}(Y_2O_3)_{0.08}O_{2-\delta}$ catalyst, and the $Ni/Ce_{0.9}Gd_{0.1}O_{2-\delta}$ catalyst exhibits the best performance.

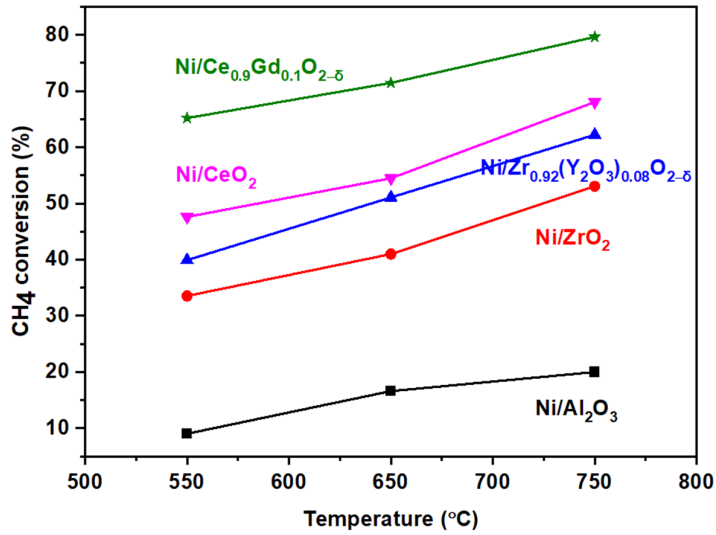


Figure 6. CH_4 conversion of the catalysts during the POM at a gas flow rate of 300 mL·min^{-1}.

As shown in Figure 7a, all catalysts reached equilibrium after 2 h of reaction. The initial activity decrease in the Ni/Al_2O_3 catalyst is attributed to the strong interaction between Ni and the support, which causes the reoxidation of part of the Ni into $NiAl_2O_4$ [4,21]. The initial activity of the other catalysts all increased, which is related to the redox process of Ni catalysts [7]. The $Ni/Ce_{0.9}Gd_{0.1}O_{2-\delta}$ catalyst achieves a high CH_4 conversion of approximately 78.6% at a gas flow rate of 300 mL·min^{-1} and 750 °C. The test results further confirm that the activity order of the catalysts is as follows: $Ni/Ce_{0.9}Gd_{0.1}O_{2-\delta}$ > Ni/CeO_2 > $Ni/Zr_{0.92}(Y_2O_3)_{0.08}O_{2-\delta}$ > Ni/ZrO_2 > Ni/Al_2O_3. Figure 7b illustrates the effect of catalysts with different supports on the H_2/CO ratio, which increases with the enhancement of OSC. This may be attributed to the improved reactivity of the water-gas shift (WGS) reaction [26]. CO adsorbed on Ni is oxidized by mobile oxygen in the support, and the mobile oxygen is subsequently reoxidized by H_2O. Higher OSC helps to enhance the reactivity of the WGS reaction, thereby achieving a higher H_2/CO ratio.

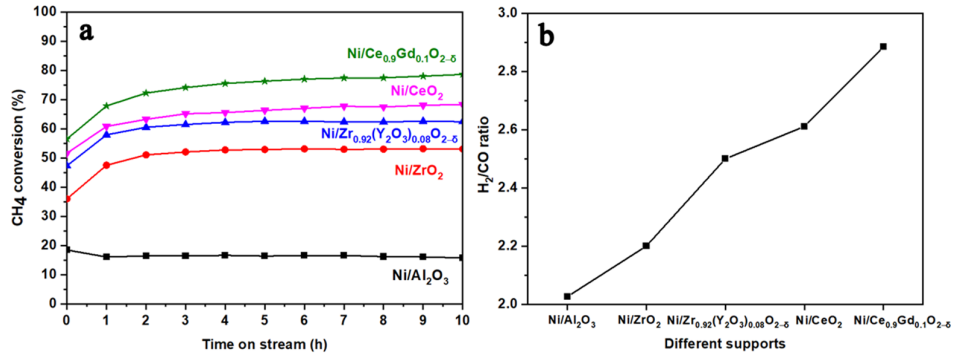


Figure 7. 10 h stability test (**a**) and H_2/CO ratio (**b**). Reaction conditions: T = 750 °C, flow rate = 300 mL·min^{-1}.

2.2. Effect of Gd^{3+} Doping in $Ni/Ce_{0.9}Gd_xO_{2-\delta}$ (x = 0.1, 0.2, 0.3)

It can be seen from the above results that doping has a significant impact on the physicochemical properties of the catalyst. To investigate the mechanism by which Gd^{3+} doping in CeO_2 support affects catalytic performance, this study prepared $Ni/Ce_{0.9}Gd_xO_{2-\delta}$ (x = 0.1, 0.2, 0.3) catalysts by adjusting the Gd^{3+} doping content. Among them, x = 0.1 corresponds

to the stoichiometric composition of the $Ce_{0.9}Gd_{0.1}O_{2-\delta}$ (GDC) support, and the other catalysts are with excessive Gd^{3+} doping.

2.2.1. Characterization of Catalysts

XRD results in Figure S1 indicate that, for the stoichiometrically Gd^{3+}-doped $Ni/Ce_{0.9}Gd_{0.1}O_{2-\delta}$ (x = 0.1) catalyst, the characteristic peak intensities of GDC and NiO are the lowest, suggesting that this catalyst has the smallest overall crystal size. However, for the excessive doping of Gd^{3+}, the crystal size of the catalyst increases again, and the crystal size of Ni after reduction also increases accordingly. This indicates that pure Gd element cannot inhibit grain growth, while the formed GDC phase is the fundamental reason for suppressing grain growth. EDS results (Figure 8) more intuitively confirm that the $Ni/Ce_{0.9}Gd_{0.1}O_{2-\delta}$ catalyst exhibits the optimal Ni dispersion. As the Gd^{3+} doping content increases, Ni particles tend to sinter and grow more readily, resulting in decreased Ni dispersion—which is consistent with the XRD results. Excessive Gd^{3+} doping triggers oxygen vacancy clustering, leading to a significant reduction in the OSC of the support (Figure S2, Table 2). In addition, Ni aggregation caused by excessive Gd^{3+} doping increases the reduction temperature (Figure S3), thereby reducing the catalyst reducibility (Table 2).

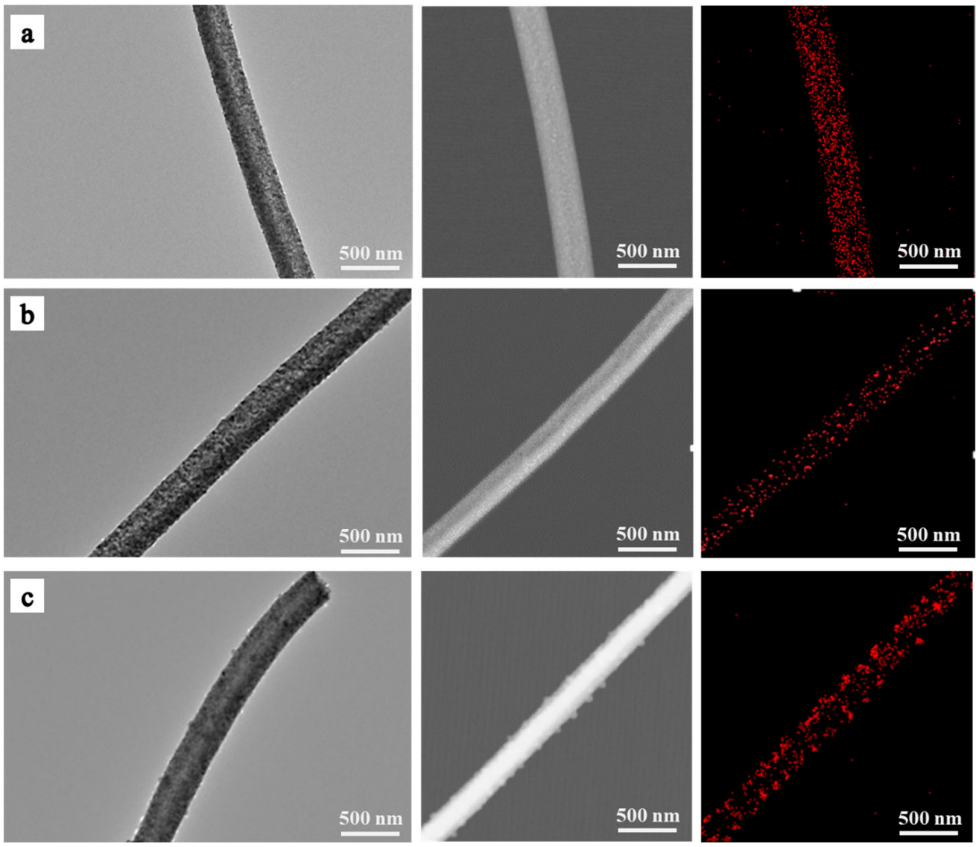


Figure 8. TEM images (**left**) and corresponding EDS Ni mapping (**right**) of reduced catalysts with different Gd^{3+} doping contents: (**a**) $Ni/Ce_{0.9}Gd_{0.1}O_{2-\delta}$; (**b**) $Ni/Ce_{0.9}Gd_{0.2}O_{2-\delta}$; (**c**) $Ni/Ce_{0.9}Gd_{0.3}O_{2-\delta}$.

Table 2. Physicochemical properties of the $Ni/Ce_{0.9}Gd_xO_{2-\delta}$ (x = 0.1, 0.2, 0.3) catalysts.

Samples	Reducibility (%)	OSC (mmol $g^{-1}_{support}$)
$Ni/Ce_{0.9}Gd_{0.1}O_{2-\delta}$	95.5	45.1
$Ni/Ce_{0.9}Gd_{0.2}O_{2-\delta}$	78.7	23.9
$Ni/Ce_{0.9}Gd_{0.3}O_{2-\delta}$	64.0	11.7

2.2.2. Catalytic Performance

The $Ni/Ce_{0.9}Gd_{0.1}O_{2-\delta}$ catalyst exhibits the best catalytic performance due to its optimal dispersion, reducibility, and OSC. However, with the increase of Gd^{3+} doping content, the catalyst's dispersion, reducibility, and OSC all decrease, resulting in a reduction in catalytic performance (Figure 9).

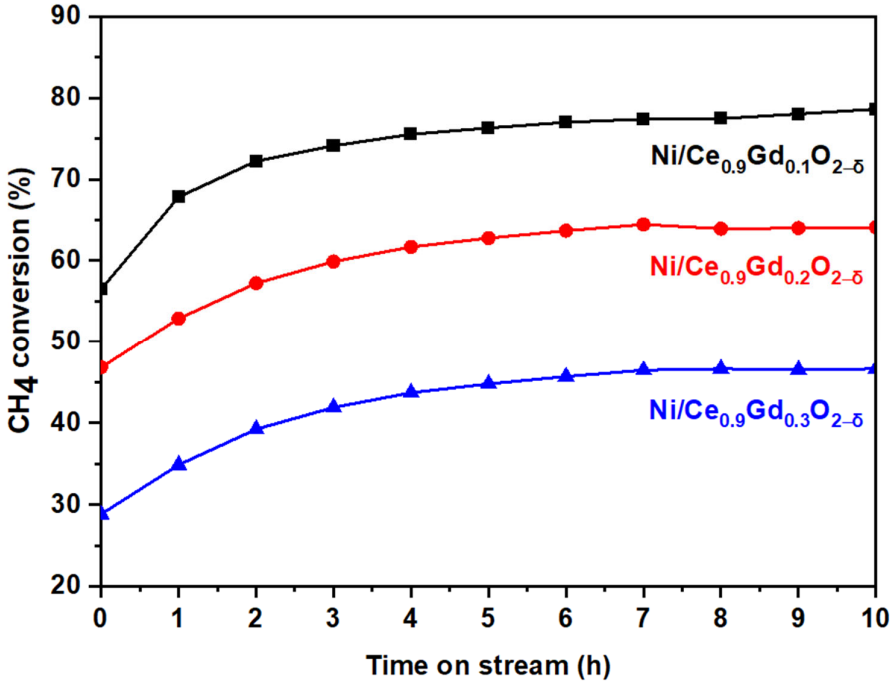


Figure 9. CH_4 conversion of the $Ni/Ce_{0.9}Gd_xO_{2-\delta}$ (x = 0.1, 0.2, 0.3) catalysts during the POM at a gas flow rate of 300 mL·min^{-1} and 750 °C.

3. Materials and Methods

3.1. Materials

Polyvinylpyrrolidone (PVP, molecular weight = 1.3×10^6) was purchased from Dibo (Shanghai, China). All nitrate reagents (purity $\geq$ 99.0 wt%) were sourced from Sinopharm Chemical Reagent Co., Ltd. (Shanghai, China).

3.2. Catalyst Preparation

All catalysts were fabricated via electrospinning, with a mixture solvent consisting of 8.0 g H_2O and 2.0 g C_2H_5OH. A total of 0.7 g PVP was incorporated into the above solvent. For the Ni/Al_2O_3, Ni/ZrO_2, and Ni/CeO_2 catalysts (each with a Ni loading of 5 wt%), their precursor solutions were formulated by dissolving $Ni(NO_3)_2{\cdot}6H_2O$ in the solvent along with $Al(NO_3)_3{\cdot}9H_2O$, $Zr(NO_3)_4{\cdot}5H_2O$, and $Ce(NO_3)_3{\cdot}6H_2O$, respectively. The precursor solution for the $Ni/Zr_{0.92}(Y_2O_3)_{0.08}O_{2-\delta}$ catalyst was prepared by mixing $Ni(NO_3)_2{\cdot}6H_2O$, $Zr(NO_3)_4{\cdot}5H_2O$, and $Y(NO_3)_3{\cdot}6H_2O$, maintaining a Ni content of 5 wt% and a Y_2O_3/ZrO_2 molar ratio of 8:92. For the $Ni/Ce_{0.9}Gd_xO_{2-\delta}$ (x = 0.1, 0.2, 0.3) catalysts, their precursor solutions were obtained by blending $Ni(NO_3)_2{\cdot}6H_2O$, $Ce(NO_3)_3{\cdot}6H_2O$, and $Gd(NO_3)_3{\cdot}6H_2O$, where x denotes the molar fraction of Gd. Notably, the Ni loading was consistently fixed at 5 wt% across all catalysts. In addition, the corresponding supports for all catalysts were fabricated via the same protocol. The electrospinning process was conducted using an electrospinning apparatus (Ucalery ET-2535H, Beijing Ucalery Industry Technology Development Co., Ltd. Beijing, China) [1], with a set spinning distance of 30 cm, driven by an applied voltage of 19 kV, and the feeding rate was stabilized at 0.05 mm·min^{-1}. The as-spun fibrous materials were subjected to stepwise heat treatment

in an air atmosphere: first, they were heated from room temperature to 400 °C at a heating rate of 1 °C min^{-1}, followed by holding at this temperature for 1 h (a critical step for degreasing and decarburization). During this process, the organic binders and carbon components were fully oxidized to CO_2 gas, which was exhausted, effectively avoiding the interference of carbon residues on the subsequent structure and performance of the catalyst. Subsequently, the materials were heated to 800 °C at a heating rate of 2 °C min^{-1} and held for 1 h; pure inorganic Ni-based metal oxide nanofibers were formed through high-temperature crystallization, completing the catalyst preparation.

4. Conclusions

This study utilizes fibrous catalysts to demonstrate that the synergistic effect of physicochemical properties—including OSC, metal–support interaction, dispersion, and reducibility—is pivotal for POM. The catalytic activity of catalysts with different supports follows the following order: $Ni/Ce_{0.9}Gd_{0.1}O_{2-\delta}$ > Ni/CeO_2 > $Ni/Zr_{0.92}(Y_2O_3)_{0.08}O_{2-\delta}$ > Ni/ZrO_2 > Ni/Al_2O_3, which is closely associated with the synergistic effect of their physicochemical properties. Among them, the $Ni/Ce_{0.9}Gd_{0.1}O_{2-\delta}$ catalyst achieves a high CH_4 conversion of approximately 78.6% at a gas flow rate of 300 mL·min^{-1} and 750 °C. Meanwhile, the $Ce_{0.9}Gd_{0.1}O_{2-\delta}$ support possesses high OSC, thereby yielding a high H_2/CO ratio of about 2.9. Doping significantly enhances Ni dispersion, reducibility, and OSC, thereby improving catalytic performance. For the $Ni/Ce_{0.9}Gd_xO_{2-\delta}$ (x = 0.1, 0.2, 0.3) catalysts, when the Gd^{3+} doping content is 0.1 at.%, the catalyst exhibits the optimal dispersion, reducibility, and OSC, corresponding to the highest catalytic performance. Increasing the Gd^{3+} doping content reduces Ni dispersion, reducibility, and OSC, thus decreasing catalytic activity. In summary, the synergistic effect of the catalyst's physicochemical properties holds decisive significance for achieving superior catalytic performance.

Supplementary Materials: The following supporting information can be downloaded at: https://www.mdpi.com/article/10.3390/catal15111090/s1, Figure S1: XRD patterns of the catalysts before (a,c) and after (b,d) reduction; Figure S2: O_2-TPD profiles of the $Ce_{0.9}Gd_xO_{2-\delta}$ (x = 0.1, 0.2, 0.3) different supports; Figure S3: TPR profiles of the $Ni/Ce_{0.9}Gd_xO_{2-\delta}$ (x = 0.1, 0.2, 0.3) catalysts.

Author Contributions: Y.M.: conceptualization, investigation, data curation, writing—original draft, writing—review and editing, supervision, project administration, funding acquisition. Y.W.: methodology, investigation. W.W.: data curation, supervision. All authors have read and agreed to the published version of the manuscript.

Funding: This research was funded by Weifang University PhD research startup foundation (Grant Nos. 2023BS31 and 2023BS35), and Weifang Science and Technology Development Plan (Grant No. 2025GX012).

Data Availability Statement: Data will be made available on request.

Conflicts of Interest: The authors declare no conflicts of interest.

References

1. Ma, Y.Y.; Ma, Y.X.; Chen, Y.; Ma, S.S.; Li, Q.G.; Hu, X.; Wang, Z.; Buckley, C.E.; Dong, D.H. Highly Stable Nanofibrous La_2NiZrO_6 Catalysts for Fast Methane Partial Oxidation. *Fuel* **2020**, *265*, 116861. [CrossRef]
2. Li, H.L.; Li, P.H.; Lin, M.; Zhu, X. Effects of $LaFeO_3$ Morphology on Oxygen Species and Chemical Looping Partial Oxidation of Methane. *Chem. Mater.* **2025**, *37*, 2931–2942. [CrossRef]
3. Shah, M. Development of Versatile Ni-Ce-Based Catalyst for Syngas Production through Dry Reforming and Catalytic Partial Oxidation of Methane. *Int. J. Hydrogen Energy* **2025**, *105*, 505–520. [CrossRef]
4. Ma, Y.Y.; Ma, Y.X.; Zhao, Z.B.; Ma, S.S.; Meng, Q.L.; Hu, X.; Buckley, C.E.; Dong, D.H. Fibrous $La_2Zr_2O_7$ Pyrochlore-Supported Ni Nanocatalysts for Methane Reforming. *J. Phys. Chem. Solids* **2020**, *147*, 109643. [CrossRef]

5. Ali, F.A.A.; Chaudhary, K.J.; Ibrahim, A.A.; Alotaibi, N.N.; Alterary, S.S.; Fadhillah, F.; Kumar, R.; Al-Fatesh, A.S. Strontium-Promoted Ni-Catalyst Supported over MgO for Partial Oxidation of Methane: Unveiling A Cost-Effective Catalyst System for Fast Mitigation of Methane. *Catalysts* **2025**, *15*, 814. [CrossRef]
6. Jang, W.J.; Shim, J.O.; Kim, H.M.; Yoo, S.Y.; Roh, H.S. A Review on Dry Reforming of Methane in Aspect of Catalytic Properties. *Catal. Today* **2019**, *324*, 15–26. [CrossRef]
7. Ma, Y.Y.; Sun, W.G.; Xie, X.Y.; Gao, Y.; Wu, X.Q.; Li, J.J.; Ye, Z.M.; Buckley, C.E.; Dong, D.H. Robust Ni Nanocatalysts Formed by Exsolution from Nanofibrous Fluorite Ceramic Supports for Methane Partial Oxidation. *Fuel* **2022**, *323*, 124442. [CrossRef]
8. Wu, G.; Zhang, C.; Li, S.; Han, Z.; Wang, T.; Ma, X.; Gong, J. Hydrogen Production via Glycerol Steam Reforming over Ni/Al_2O_3: Influence of Nickel Precursors. *ACS Sustain. Chem. Eng.* **2013**, *1*, 1052–1062. [CrossRef]
9. Salhi, N.; Boulahouache, A.; Petit, C.; Kiennemann, A.; Rabia, C. Steam Reforming of Methane to Syngas over $NiAl_2O_4$ Spinel Catalysts. *Int. J. Hydrogen Energy* **2011**, *36*, 11433–11439. [CrossRef]
10. Charisiou, N.D.; Siakavelas, G.; Tzounis, L.; Sebastian, B.D.; Hinder, S.J.; Baker, M.A.; Polychronopoulou, K.; Goula, M.A. Ni/Y_2O_3-ZrO_2 Catalyst for Hydrogen Production through the Glycerol Steam Reforming Reaction. *Int. J. Hydrogen Energy* **2020**, *45*, 10442–10460. [CrossRef]
11. Dong, W.S.; Jun, K.W.; Roh, H.S.; Liu, Z.W.; Park, S.E. Comparative Study on Partial Oxidation of Methane over Ni/ZrO_2, Ni/CeO_2 and Ni/Ce–ZrO_2 Catalysts. *Catal. Lett.* **2002**, *78*, 215–222. [CrossRef]
12. Takeguchi, T.; Furukawa, S.N.; Inoue, M. Hydrogen Spillover from NiO to the Large Surface Area CeO_2–ZrO_2 Solid Solutions and Activity of the NiO/CeO_2–ZrO_2 Catalysts for Partial Oxidation of Methane. *J. Catal.* **2001**, *202*, 14–24. [CrossRef]
13. Mikulová, J.; Sylvie, R.; Jacques, B.; Daniel, D.; Charles, K. Characterizations of Platinum Catalysts Supported on Ce, Zr, Pr-Oxides and Formation of Carbonate Species in Catalytic Wet Air Oxidation of Acetic Acid. *Catal. Today* **2007**, *124*, 185–190. [CrossRef]
14. Harshini, D.; Lee, D.; Jeong, J.; Kim, Y.; Nam, S.; Ham, H.; Han, J.; Lim, T.; Yoon, C. Enhanced Oxygen Storage Capacity of $Ce_{0.65}Hf_{0.25}M_{0.1}O_{2-\delta}$ (M = Rare Earth Elements): Applications to Methane Steam Reforming with High Coking Resistance. *Appl. Catal. B* **2014**, *148–149*, 415–423. [CrossRef]
15. Fonseca, R.O.; Garrido, G.S.; Rabelo-Neto, R.C.; Silveira, E.B.; Simões, R.C.C.; Mattos, L.V.; Noronha, F.B. Study of the Effect of Gd-Doping Ceria on the Performance of $Pt/GdCeO_2/Al_2O_3$ Catalysts for the Dry Reforming of Methane. *Catal. Today* **2020**, *355*, 737–745. [CrossRef]
16. Kim, H.; Jeong, N.J.; Han, S.O. Synthesis of A Catalytic Support from Natural Cellulose Fibers, and Its Performance in A CO_2 Reforming of CH_4. *Appl. Catal. B* **2012**, *113–114*, 116–125. [CrossRef]
17. Abdullah, B.; Abd Ghani, N.A.; Vo, D.-V.N. Recent Advances in Dry Reforming of Methane over Ni-based Catalysts. *J. Clean. Prod.* **2017**, *162*, 170–185. [CrossRef]
18. Zheng, W.T.; Sun, K.Q.; Liu, H.M.; Yu, L.; Xu, B.Q. Nanocomposite Ni/ZrO_2: Highly Active and Stable Catalyst for H_2 Production via Cyclic Stepwise Methane Reforming Reactions. *Int. J. Hydrogen Energy* **2012**, *37*, 11735–11747. [CrossRef]
19. Ma, Y.Y.; Ma, Y.X.; Zhao, Z.B.; Hu, X.; Ye, Z.M.; Yao, J.F.; Buckley, C.E.; Dong, D.H. Comparison of fibrous catalysts and monolithic catalysts for catalytic methane partial oxidation. *Renew. Energy* **2019**, *138*, 1010–1017. [CrossRef]
20. Montoya, J.A.; Romero-Pascual, E.; Gimon, C.; Angel, P.D.; Monzon, A. Methane Reforming with CO_2 over Ni/ZrO_2-CeO_2 Catalysts Prepared by Sol-Gel. *Catal. Today* **2000**, *63*, 71–85. [CrossRef]
21. Ma, Y.Y.; Ma, Y.X.; Liu, M.; Chen, Y.; Hu, X.; Ye, Z.M.; Dong, D.H. Study on Nanofibrous Catalysts Prepared by Electrospinning for Methane Partial Oxidation. *Catalysts* **2019**, *9*, 479. [CrossRef]
22. Bellido, J.D.A.; Assaf, E.M. Effect of the Y_2O_3–ZrO_2 Support Composition on Nickel Catalyst Evaluated in Dry Reforming of Methane. *Appl. Catal. A-Gen.* **2009**, *352*, 179–187. [CrossRef]
23. Yang, C.; Zhang, J.P.; Wang, J.K.; Li, D.F.; Li, K.Z.; Zhu, X. Oxygen Vacancies Enriched $Ni-Co/SiO_2@CeO_2$ Redox Catalyst for Cycling Methane Partial Oxidation and CO_2 Splitting. *Chin. J. Chem. Eng.* **2023**, *63*, 235–245. [CrossRef]
24. Zhang, M.; Zhang, J.; Zhou, Z.; Chen, S.; Zhang, T.; Song, F.; Zhang, Q.; Tsubaki, N.; Tan, Y.; Han, Y. Effects of the Surface Adsorbed Oxygen Species Tuned by Rare-Earth Metal Doping on Dry Reforming of Methane over Ni/ZrO_2 Catalyst. *Appl. Catal. B* **2020**, *264*, 118522. [CrossRef]
25. Morales, M.; Piñol, S.; Segarra, M. Intermediate Temperature Single-Chamber Methane Fed SOFC Based on Gd Doped Ceria Electrolyte and $La_{0.5}Sr_{0.5}CoO_{3-1}$ as Cathode. *J. Power Sources* **2009**, *194*, 961–966. [CrossRef]
26. Cao, L.; Ni, C.; Yuan, Z.; Wang, S. Correlation between Catalytic Selectivity and Oxygen Storage Capacity in Autothermal Reforming of Methane over $Rh/Ce_{0.45}Zr_{0.45}RE_{0.1}$ Catalysts (RE = La, Pr, Nd, Sm, Eu, Gd, Tb). *Catal. Commun.* **2009**, *10*, 1192–1195. [CrossRef]
27. Takano, H.; Kirihata, Y.; Izumiya, K.; Kumagai, N.; Hashimoto, K. Highly Active Ni/Y-Doped ZrO_2 Catalysts for CO_2 Methanation. *Appl. Surf. Sci.* **2015**, *388*, 653–663. [CrossRef]
28. Kumar, R.; Kumar, K.; Choudary, N.V.; Pant, K.K. Effect of Support Materials on the Performance of Ni-Based Catalysts in Tri-Reforming of Methane. *Fuel Process. Technol.* **2019**, *186*, 40–52. [CrossRef]

29. Pizzolitto, C.; Pupulin, E.; Menegazzo, F.; Ghedini, E.; Michele, A.D.; Mattarelli, M.; Cruciani, G.; Signoretto, M. Nickel Based Catalysts for Methane Dry Reforming: Effect of Supports on Catalytic Activity and Stability. *Int. J. Hydrogen Energy* **2019**, *44*, 28065–28076. [CrossRef]
30. Dai, Y.; Liu, W.; Formo, E.; Sun, Y.; Xia, Y. Ceramic Nanofibers Fabricated by Electrospinning and Their Applications in Catalysis, Environmental Science, and Energy Technology. *Polym. Adv. Technol.* **2011**, *22*, 326–338. [CrossRef]
31. Wang, Z.T.; Hu, X.; Dong, D.H.; Parkinson, G.; Li, C.Z. Effects of Calcination Temperature of Electrospun Fibrous Ni/Al_2O_3 Catalysts on the Dry Reforming of Methane. *Fuel Process. Technol.* **2017**, *155*, 246–251. [CrossRef]
32. Wang, Z.T.; Cheng, Y.; Shao, X.; Veder, J.-P.; Hu, X.; Ma, Y.Y.; Wang, J.J.; Xie, K.; Dong, D.H.; Jiang, S.P. Nanocatalysts Anchored on Nanofiber Support for High Syngas Production via Methane Partial Oxidation. *Appl. Catal. A-Gen.* **2018**, *565*, 119–126. [CrossRef]
33. Lofberg, A.; Guerrero-Caballero, J.; Kane, T.; Rubbens, A.; Jalowiecki-Duhamel, L. Ni/CeO_2 Based Catalysts as Oxygen Vectors for the Chemical Looping Dry Reforming of Methane for Syngas Production. *Appl. Catal. B* **2017**, *212*, 159–174. [CrossRef]
34. Singha, R.K.; Shukla, A.; Yadav, A.; Konathala, L.N.S.; Bal, R. Effect of Metal-Support Interaction on Activity and Stability of Ni-CeO_2 Catalyst for Partial Oxidation of Methane. *Appl. Catal. B-Environ.* **2017**, *202*, 473–488. [CrossRef]
35. Zou, Q.; Zhao, Y.H.; Jin, X.; Fang, J.; Li, D.Y.; Li, K.Z.; Lu, J.C.; Luo, Y.M. Ceria-Nano Supported Copper Oxide Catalysts for CO Preferential Oxidation: Importance of Oxygen Species and Metal-Support Interaction. *Appl. Surf. Sci.* **2019**, *494*, 1166–1176. [CrossRef]

Disclaimer/Publisher's Note: The statements, opinions and data contained in all publications are solely those of the individual author(s) and contributor(s) and not of MDPI and/or the editor(s). MDPI and/or the editor(s) disclaim responsibility for any injury to people or property resulting from any ideas, methods, instructions or products referred to in the content.